

Article

Transformation Induced Plasticity Effects of a Non-Equal Molar Co-Cr-Fe-Ni High Entropy Alloy System

Wei Fang^{1,2}, Ruobin Chang¹, Puguang Ji¹, Xin Zhang^{1,*}, Baoxi Liu¹, Xuanhui Qu³  and Fuxing Yin^{1,2,*}

¹ Research Institute for Energy Equipment Materials, School of Materials Science and Engineering, Hebei University of Technology, Tianjin 300132, China; fangwei@hebut.edu.cn (W.F.); changruobin@163.com (R.C.); jipuguang@hebut.edu.cn (P.J.); liubaoxiliubo@126.com (B.L.)

² Tianjin Key Laboratory of Materials Laminating Fabrication and Interface Control Technology, Tianjin 300132, China

³ State Key Laboratory for Advance Metals and Materials, University of Science and Technology Beijing, Beijing 10083, China; quxh@ustb.edu.cn

* Correspondence: zhang_xin@hebut.edu.cn (X.Z.); yinfuxing@hebut.edu.cn (F.Y.)

Received: 27 April 2018; Accepted: 18 May 2018; Published: 21 May 2018



Abstract: Metastability-engineering strategy is an important topic for high entropy alloys (HEAs), owing to the transformation-induced plasticity effect (TRIP). In this work, TRIP effects of Co-Cr-Fe-Ni HEAs are investigated. Results indicate the tensile deformation-induced martensitic transformation occurs in $\text{Co}_{35}\text{Cr}_{25}\text{Fe}_{40-x}\text{Ni}_x$ ($x = 0\text{--}15$ at %) HEAs. The excellent combination of tensile strength (760 MPa–1000 MPa) and elongation (65–35%) owe to solid solution strengthening of Co and Cr, and the TRIP effect. In non-equal molar Co-Cr-Fe-Ni systems, with the decrease of Ni content, the values of stacking fault energy (SFE) decrease; thus, TRIP phenomena occurs. Based on the experimental investigation in three different regions of the Co-Cr-Fe-Ni multicomponent phase diagram, the face-centered cubic structured Co-Cr-Fe-Ni HEAs with VEC of ~ 8.0 is more metastable, and TRIP phenomena are more likely to occur.

Keywords: high entropy alloys; metastability; transformation induced plasticity effect; valence electron concentration; stacking fault energy

1. Introduction

High entropy alloys (HEAs), or multi-principal-component alloys [1] show remarkable properties, mainly for their twinning induced plasticity (TWIP) effect [2], or transformation induced plasticity (TRIP) effect [3], due to overcoming the strength-ductility trade-off in the composition design of alloys. Generally, low stacking fault energy (SFE) HEAs with face-centered cubic (FCC) single phases are more likely to deform by twinning, with increased strain hardening rates [2,4–6]. With the decreasing temperature, the very low SFE values at cryogenic conditions suggest that the possible presence of the TRIP effect via ab initio calculations [7]. Nano-twins and hexagonal close packed (HCP) lamellae are observed to coexist in CoCrNi at 77 K, suggesting a possible evolution of the deformation mechanism from nano-twinning to phase transformation in equal molar CoCrNi [8]. Usually, the SFE of HEAs were experimentally measured by weak-beam dark-field transmission electron microscopy [5,9] or theoretically calculated by first principles calculations, such as the exact muffin-tin orbitals (EMTO) method [7,10].

CoCrNi alloy exhibits an excellent combination of strength and ductility—greater than that of CoCrFeMnNi alloy at both cryogenic and room temperatures [5]. This indicates that stronger alloys are

not necessarily those with the most elements [11]. The Co diffusivity is higher in CoCrFeMnNi than in CoCrFeNi above 1020 K, which suggests that diffusion in HEAs need not be assumed to decrease with an increasing number of elements [12]. It is a challenge to design the proportions of the various elements necessary to obtain better mechanical properties in non-equal molar HEAs based on the nature of the constituent elements. Li et al. [3,13–15] reported a series of TRIP-dual phase-HEAs, such as $\text{Co}_{10}\text{Cr}_{10}\text{Fe}_{80-x}\text{Mn}_x$, $\text{Co}_{20}\text{Cr}_{20}\text{Fe}_{40-x}\text{Mn}_{20}\text{Ni}_x$. Ab initio calculations also play an important role in HCP-FCC phase stability analyses on Ni content. Simulation results indicate that enhanced HCP phase stability with reduced Ni concentration is beneficial for the appearance of TRIP phenomena in HEAs systems, which helps to obtain the excellent combination of strength and ductility [13]. However, few HEAs systems with the TRIP effects have been reported. Therefore, it is necessary to develop a new class of TRIP assisted HEAs.

It is worth noting that phase stability in HEAs with FCC single phase solid solutions is relative, or conditional. A polymorphic transition from FCC to HCP occurs in the CoCrFeMnNi under hydrostatic compression at room temperature, and the transition is irreversible, which reveals that the FCC phase is a stable polymorph at high temperatures, while the HCP structure is more thermodynamically favorable at lower temperatures [16]. The Cr-rich sigma phase forms at grain boundaries of CoCrFeMnNi HEAs following prolonged exposures at 700 °C [17,18]. A small amount of added Al accelerates the composition and decomposition, and induces the instability of $\text{Al}_{0.1}\text{CoCrFeNi}$ HEAs in long duration annealed conditions [19]. These phenomena indicate that HEAs are metastable, and that the addition of certain elements increases their metastability. The valence electron concentration (VEC) is a useful criterion for phase prediction. At $\text{VEC} \geq 8.0$, a sole FCC solid-solution phase is formed. At $\text{VEC} < 6.87$, a sole BCC solid-solution phase exists. And when $6.87 \leq \text{VEC} < 8$, both the FCC and BCC phases will coexist [20], noting that the FCC single phase HEAs with VEC of ~ 8.0 is more metastable. In the present study, the TRIP effect in non-equal molar Co-Cr-Fe-Ni systems was investigated, and the relationships among the VEC, SFE and TRIP effects were discussed.

2. Experimental Methods

$\text{Co}_{35}\text{Cr}_{25}\text{Fe}_{40-x}\text{Ni}_x$ ($x = 15$ at %, 10 at %, 5 at %, 0 at %), named as Ni-15, Ni-10, Ni-5, Ni-0, and $\text{Co}_{30}\text{Cr}_{30}\text{Fe}_{25}\text{Ni}_{15}$, and $\text{Co}_{20}\text{Cr}_{25}\text{Fe}_{45}\text{Ni}_{10}$ are selected to investigate the correlation of the VEC, SFE and TRIP phenomena, compared with the previous investigation of $\text{Co}_x\text{Cr}_{25}\text{Fe}_{50-x}\text{Ni}_{25}$ with the TWIP phenomena [21]. Alloy ingots were prepared by arc-melting using the constituent pure metals (>99.9% pure) under an Ar atmosphere, and were subsequently homogenized at 1200 °C for 4 h. Then, the samples were warm-rolled at 700 °C by 70% reduction, and annealed at 900 °C for 10 min, followed by water quenching. The dog bone-shaped tensile samples were prepared with a gauge length 10 mm, a width 5 mm, and a thickness 1.2 mm. A SHIMADZU AGS universal electronic tensile testing machine was employed for tensile tests at room temperature with a nominal strain rate of 10^{-3} s^{-1} . X-ray diffraction (XRD) measurements were performed using a Bruker D8 DISCOVER equipped with Cu $K\alpha$ radiation, operating at 40 kV and 40 mA, between 30° and 100° (2 θ), with step size 3°/min, before and after the tensile test. Electron backscatter diffraction (EBSD) measurements were carried out using the JEOL 7100F SEM equipped with the TSL OIM data collection software. JEOL 8530F electron probe microanalysis (EPMA) measurements were used to obtain composition and for elements mapping of micro area. For the microstructural measurements, samples were electrically polished in a solution of 20% HClO_4 and 80% $\text{C}_2\text{H}_5\text{OH}$ at 25 V for 60 s at 273 K, after mechanical polishing.

3. Results and Discussions

3.1. Strain Induced Phase Transformation

Chemical compositions of $\text{Co}_{35}\text{Cr}_{25}\text{Fe}_{40-x}\text{Ni}_x$, measured by wavelength-dispersive spectroscopy, are shown in Table 1. The measured compositions of four alloys are close to the nominal compositions.

VEC for a multi-component alloy is defined as $VEC = \sum_{i=1}^n c_i(VEC)_i$, where c_i and $(VEC)_i$ are the atomic percentage, and VEC for the individual element. The VEC of element Co, Cr, Fe and Ni are 9, 6, 8 and 10, respectively. The values of VEC of Ni-15, Ni-10, Ni-5, Ni-0 are 8.15, 8.05, 7.95 and 7.85, respectively. Figure 1 presents the XRD patterns of $Co_{35}Cr_{25}Fe_{40-x}Ni_x$ ($x = 15$ at %, 10 at %, 5 at %, 0 at %) HEAs before and after tensile test. A single FCC phase was obtained when the Ni content is at 15% (Ni-15, VEC = 8.15). With further decrease of Ni content in the $Co_{35}Cr_{25}Fe_{40-x}Ni_x$, the structure of the HEAs shifts from single FCC phase to FCC, and HCP dual phase. Note that the minor HCP phase was thermally induced during the water quenching, after the 900 °C annealing process, in Ni-5 and Ni-0, with VEC of 7.95 and 7.85. The XRD results of tensile tested samples show that FCC and HCP phase are both observed in all the four alloys, which indicates that the deformation-induced martensitic transformation (FCC \rightarrow HCP) is a primary deformation mechanism. The intensities of FCC peaks decrease, while those of the HCP peaks increase significantly, indicating that the volume fraction of HCP phase increases after the tensile deformation with the decreasing Ni content. Figure 2 shows the EBSD phase maps of annealed samples and fractured samples of $Co_{35}Cr_{25}Fe_{40-x}Ni_x$ ($x = 15$ at %, 10 at %, 5 at %, 0 at %) HEAs. The results indicate that a ~ 3 vol % thermally induced HCP phase exists in the annealed Ni-10 sample, with VEC of 8.05, which is not captured in the XRD results. Meanwhile, ~ 10 vol % and ~ 30 vol % HCP phase exists in the annealed Ni-5 and Ni-0 samples, with VEC of 7.95 and 7.85, which is consistent with the XRD results in Figure 1a, noting that the volume fraction of thermally induced HCP phase increased with the disappearance of annealing twins. Based on EBSD phase maps of fractured samples of $Co_{35}Cr_{25}Fe_{40-x}Ni_x$ HEAs in Figure 2, deformation induced HCP phases were observed in all four alloys. The volume fractions of HCP phase of Ni-15, Ni-10, Ni-5, Ni-0 are $\sim 45\%$, $\sim 66\%$, $\sim 76\%$ and 85%, respectively, which follow the same trend as the XRD results in Figure 1b. The HCP phase is formed in the FCC matrix, and mainly exhibits laminate morphology; some thin HCP laminates are also exhibited, as shown in Figure 3. The results show that all elements are uniformly distributed in $Co_{35}Cr_{25}Fe_{40}$ with FCC and HCP dual-phase. Combining the XRD and EBSD analyses, we confirm that the stability of the FCC phase is lower, that the thermally induced HCP phase occurs with the decrease of Ni content when the $VEC \leq 8.05$, and that the deformation-induced HCP phase occurs in all the four alloys.

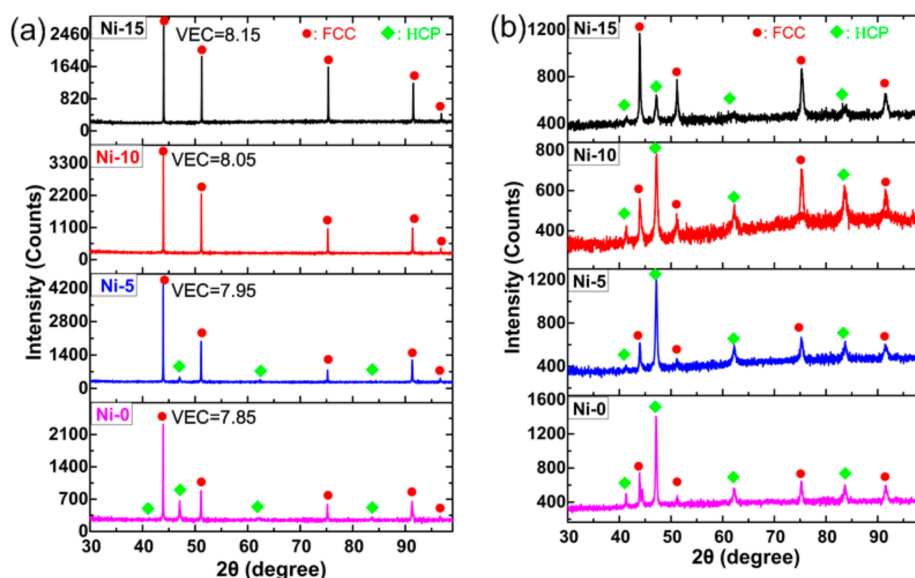


Figure 1. XRD patterns of $Co_{35}Cr_{25}Fe_{40-x}Ni_x$ ($x = 15$ at %, 10 at %, 5 at %, 0 at %) HEAs before (a) and after (b) tensile test.

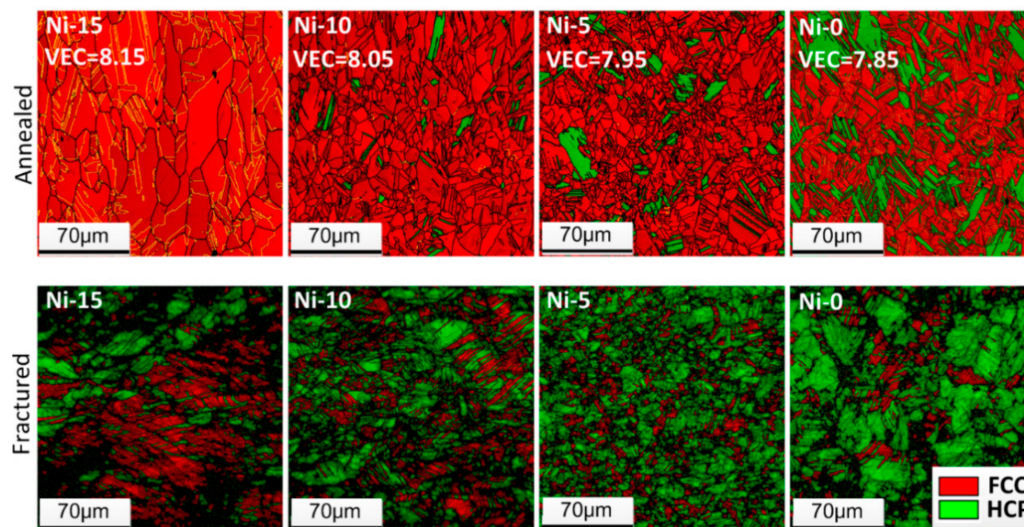


Figure 2. EBSD phase maps of annealed samples and fractured samples of $\text{Co}_{35}\text{Cr}_{25}\text{Fe}_{40-x}\text{Ni}_x$ ($x = 15$ at %, 10 at %, 5 at %, 0%) HEAs. The black lines and yellow lines indicate grain boundaries and twin boundaries (For interpretation of the references to color in this figure legend, the reader is referred to the web version of this article).

Table 1. Chemical compositions of HEAs (at %) measured by wavelength-dispersive spectroscopy.

Alloys	Co	Cr	Fe	Ni	VEC
$\text{Co}_{35}\text{Cr}_{25}\text{Fe}_{25}\text{Ni}_{15}$	34.7 ± 0.3	25.4 ± 0.2	25.1 ± 0.1	14.8 ± 0.2	8.15
$\text{Co}_{35}\text{Cr}_{25}\text{Fe}_{30}\text{Ni}_{10}$	34.8 ± 0.2	25.3 ± 0.2	30.2 ± 0.1	9.7 ± 0.1	8.05
$\text{Co}_{35}\text{Cr}_{25}\text{Fe}_{35}\text{Ni}_5$	34.8 ± 0.2	25.4 ± 0.3	35.1 ± 0.2	4.7 ± 0.1	7.95
$\text{Co}_{35}\text{Cr}_{25}\text{Fe}_{40}\text{Ni}_0$	34.7 ± 0.2	25.2 ± 0.3	40.1 ± 0.1	0	7.85

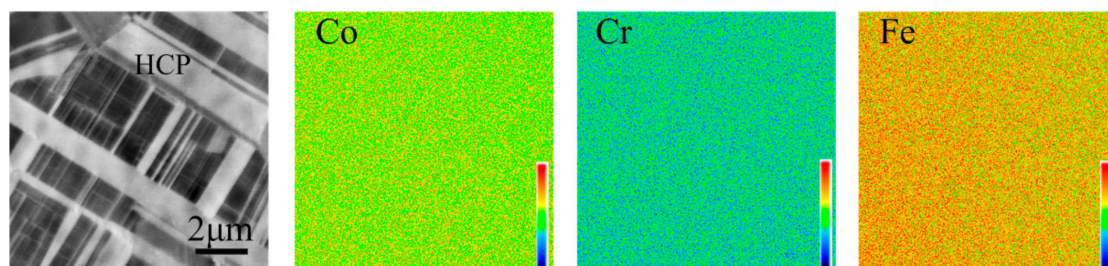


Figure 3. EPMA maps of the $\text{Co}_{35}\text{Cr}_{25}\text{Fe}_{40}$ alloy annealed at $900\text{ }^\circ\text{C}$. Lath-like microstructure is HCP phase. Show that all elements (Co, Cr and Fe) are uniformly distributed in $\text{Co}_{35}\text{Cr}_{25}\text{Fe}_{40}$.

3.2. Mechanical Properties

Figure 4 shows the representative tensile stress-strain curves of the Ni-15, Ni-10, Ni-5, and Ni-0. With the decrease of Ni content from 15% to 5%, the ultimate tensile strength increases from 760 MPa to 1000 MPa, and the total elongation decreases from 65% to 35%. As mentioned above, the initial HCP phase volume fraction of Ni-15 and Ni-0 are 0% and 30%, respectively. Meanwhile, the stability of the FCC phase of Ni-0 is lowest among the four alloys, which means that the rate of phase transformation of Ni-0 is relatively high, and that transformation capacity will be consumed already at a modest strain level [13,15], resulting in the lowest elongation of the four alloys. The phenomenon is similar to the reported results of $\text{Co}_{20}\text{Cr}_{20}\text{Fe}_{40-x}\text{Mn}_{20}\text{Ni}_x$ ($x = 0\text{--}20$ at %) HEAs [13], but the strength is higher in the $\text{Co}_{35}\text{Cr}_{25}\text{Fe}_{40-x}\text{Ni}_x$ HEAs, owing to the solid solution strengthening through the higher content of elements Co and Cr. Interestingly, the strength of $\text{Co}_{35}\text{Cr}_{25}\text{Fe}_{40-x}\text{Ni}_x$ HEAs is enhanced with a decrease of Ni content or VEC of alloys, while ductility is improved with an increase of Ni content

or VEC of alloys, which is similar to the proposed strategy to balance the strength and ductility of FCC-BCC dual phase HEAs based upon the VEC [22]. In summary, the deformation induced martensitic transformation is a primary deformation mechanism, and the TRIP effect is the main reason for the good strength and ductility combination in the four alloys.

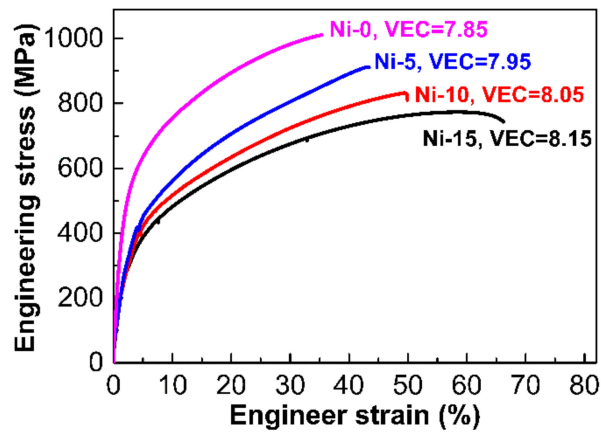


Figure 4. Mechanical behavior of the $\text{Co}_{35}\text{Cr}_{25}\text{Fe}_{40-x}\text{Ni}_x$ ($x = 15$ at %, 10 at %, 5 at %, 0%) HEAs.

3.3. The Correlation among SFE, VEC and TRIP Effect in Co-Cr-Fe-Ni System

Previous studies indicate that TRIP effects are mainly determined by SFE [15], which can be expressed as Equation (1).

$$\text{SFE} = 2\rho\Delta G^{\text{FCC}\rightarrow\text{HCP}} + 2E^{\text{FCC}\rightarrow\text{HCP}}, \quad (1)$$

where ρ is the planar packing density of a close packed plane. $\Delta G^{\text{FCC}\rightarrow\text{HCP}}$ is the molar free energy difference between the FCC and HCP phase, and $E^{\text{FCC}\rightarrow\text{HCP}}$ is the coherent FCC-HCP interfacial energy. For a certain alloy system of transition metal FCC HEAs, if the planar packing density and coherent FCC-HCP interfacial energy are similar, then the SFE is mainly determined by the free energy difference between the FCC and HCP phases.

For the HEAs which are mainly constituted of transition metals, the integration of the density of states actually results in VEC, which includes not only s- and p-electrons, but d-electrons, forming the valance band, based on the First principles band calculations [23]. Our results indicate that VEC is useful to study the electron concentration effect on the phase stability in Co-Cr-Fe-Ni HEAs. The FCC phase HEAs with a VEC of ~ 8.0 is more metastable, which means that the HCP phase energies are generally lower than those of FCC phase, and that TRIP phenomena are more likely to occur.

To verify the correlation among TRIP effects, SFE and VEC of HEAs, another two alloys in different regions of multicomponent phase diagram, are designed as $\text{Co}_{30}\text{Cr}_{30}\text{Fe}_{25}\text{Ni}_{15}$, $\text{Co}_{20}\text{Cr}_{25}\text{Fe}_{45}\text{Ni}_{10}$, with VEC of 8.0 and 7.9, respectively. As shown in Figure 5, deformation-induced martensitic transformation occurs in both two alloys. The higher Co and Cr content improves strength. But there is no thermally induced HCP phase in these two alloys, which is different from the Ni-10 with VEC of 8.05, indicating that the phase stability of non-equal Co-Cr-Fe-Ni HEA is different, even with the same VEC value of designed compositions. The VEC of equal molar CoCrFeNi HEA is 8.25. The calculated SFEs of Fe-Cr-Ni austenitic stainless steels, with respect to the Ni content [10,24], are shown in Figure 6. The stacking fault energies always decrease with a decreasing Ni content in Fe-Cr-Ni austenitic stainless steels [10,24], which is similar to FCC-structured Co-Cr-Fe-Ni alloy systems. Therefore, with the decrease of Ni content, the VEC of Co-Cr-Fe-Ni system decreases, and the SFEs are more likely to decrease sharply, based on the first principles study [10,24]. As a whole, phase transformation is more likely to occur with a VEC between 7.8 and 8.1 in non-equal Co-Cr-Fe-Ni HEAs, which means relatively low values of SFE.

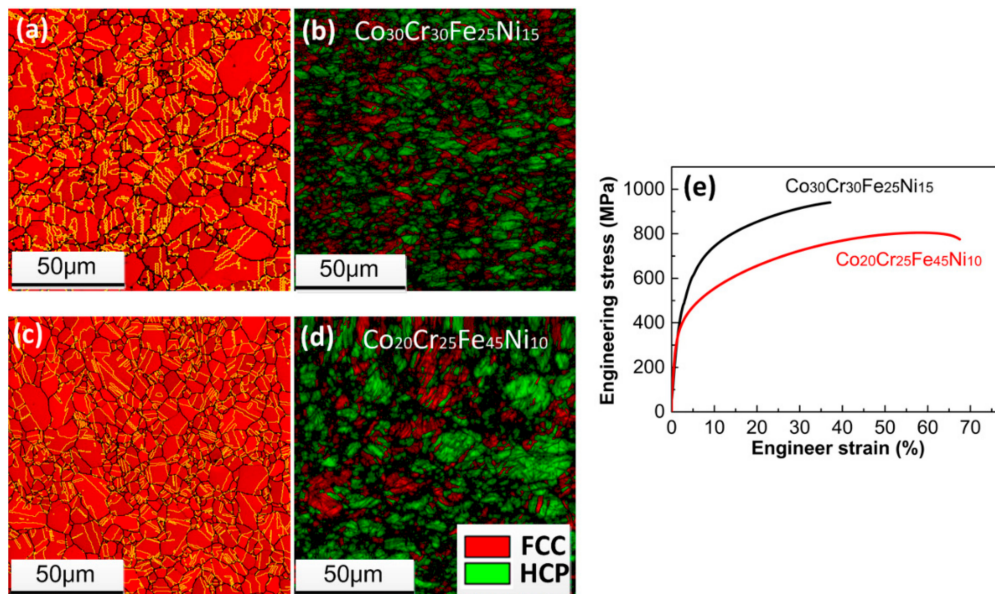


Figure 5. EBSD phase maps of HEAs, annealed sample (a) and fractured sample (b) of $\text{Co}_{30}\text{Cr}_{30}\text{Fe}_{25}\text{Ni}_{15}$ with the VEC of 8.0; annealed sample (c) and fractured sample (d) of $\text{Co}_{20}\text{Cr}_{25}\text{Fe}_{45}\text{Ni}_{10}$ with the VEC of 7.9. The black lines and yellow lines indicate grain boundaries and twin boundaries. (e) stress-strain curves of the two alloys (For interpretation of the references to color in this figure legend, the reader is referred to the web version of this article).

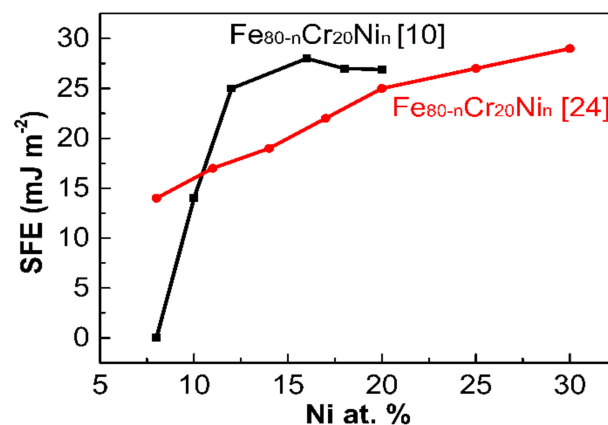


Figure 6. The calculated SFE of Fe-Cr-Ni austenitic stainless steels with respect to the Ni content in references [10,24].

3.4. Plastic Deformation Mechanism Transition

The TWIP and TRIP phenomena are mainly determined by the SFE [25]. The ability to predict the phase metastability from fundamental properties of constituent elements would benefit the alloy design greatly [20]. VEC was used to study the electron concentration effect on the phase stability in HEAs, which is found to be helpful for alloy design [20]. As mentioned above, TRIP phenomena are more likely to occur with a VEC of between 7.8 and 8.1, in non-equal Co-Cr-Fe-Ni HEAs. Further, in order to investigate the effect of VEC on TWIP and TRIP phenomena in universal HEAs, the composition and VEC of reported HEAs with TWIP and TRIP phenomena are summarized in Table 2.

Table 2. Composition and VEC of reported HEAs with TWIP and TRIP phenomena.

Alloys	VEC	Dominated Mechanism	Ref.
Co ₃₅ Cr ₂₅ Fe ₁₅ Ni ₂₅	8.35	TWIP	[21]
Co ₃₀ Cr ₂₅ Fe ₂₀ Ni ₂₅	8.3	TWIP	[21]
Co ₂₅ Cr ₂₅ Fe ₂₅ Ni ₂₅	8.25	TWIP	[21]
Co ₂₀ Cr ₂₅ Fe ₃₀ Ni ₂₅	8.2	TWIP	[21]
Co ₃₅ Cr ₂₅ Fe ₂₅ Ni ₁₅	8.15	TRIP	this work
Co ₃₅ Cr ₂₅ Fe ₃₀ Ni ₁₀	8.05	TRIP	this work
Co ₃₅ Cr ₂₅ Fe ₃₅ Ni ₅	7.95	TRIP	this work
Co ₃₅ Cr ₂₅ Fe ₄₀ Ni ₀	7.85	TRIP	this work
Co ₃₀ Cr ₃₀ Fe ₂₅ Ni ₁₅	8	TRIP	this work
Co ₂₀ Cr ₂₅ Fe ₄₅ Ni ₁₀	7.9	TRIP	this work
Co _{33.3} Cr _{33.3} Ni _{33.3}	8.33	TWIP+HCP lamellae *	[8]
Co _{33.3} Cr _{33.3} Ni _{33.3}	8.33	TWIP	[5]
Co ₂₀ Cr ₂₀ Fe ₂₀ Mn ₂₀ Ni ₂₀	8.0	TWIP	[5]
Co ₂₀ Cr ₂₀ Fe ₂₀ Mn ₂₀ Ni ₂₀	8	TWIP	[13]
Co ₂₀ Cr ₂₀ Fe ₃₄ Mn ₂₀ Ni ₆	7.72	TRIP	[13]
Co ₂₀ Cr ₂₀ Fe ₄₀ Mn ₂₀ Ni ₀	7.6	TRIP	[13]
Co ₁₀ Cr ₁₀ Fe ₃₅ Mn ₄₅	7.45	Dislocation slip	[3]
Co ₁₀ Cr ₁₀ Fe ₄₀ Mn ₄₀	7.5	TWIP	[3,26]
Co ₁₀ Cr ₁₀ Fe ₄₅ Mn ₃₅	7.55	TRIP	[3]
Co ₁₀ Cr ₁₀ Fe ₅₀ Mn ₃₀	7.6	TRIP	[3]
Co _{23.6} Cr _{23.6} Fe _{23.6} Ni _{23.6} Mo _{5.6}	8.12	TWIP	[27]
Co _{24.3} Cr _{24.3} Fe _{24.3} Ni _{24.3} Al _{2.8}	8.12	TWIP	[28]
Co _{23.3} Cr _{23.3} Fe _{23.3} Ni _{23.3} Al _{6.8}	7.89	TWIP	[29,30]

* At the cryogenic temperature.

TWIP phenomena occur in Co_xCr₂₅Fe_{50-x}Ni₂₅ (x = 20–35 at %) with VEC between 8.35 and 8.2 [21]. Then, when the VEC < 8.2, TRIP phenomena occur in Co₃₅Cr₂₅Fe_{40-x}Ni_x (x = 0–15 at %), Co₃₀Cr₃₀Fe₂₅Ni₁₅ and Co₂₀Cr₂₅Fe₄₅Ni₁₀, owing to the increase of metastability. TWIP phenomena were observed in the equal molar Co_{33.3}Cr_{33.3}Ni_{33.3} alloy with SFE of ~22 mJ/m² and VEC of 8.33 [5,8]. But at the cryogenic temperature, a new phase with HCP lamellae also appeared, suggesting a possible evolution from TWIP to TRIP, because the HCP phase is indeed energetically favorable relative to FCC phase at 0 K, based on the first principles calculations [8,31]. It is worth noting that the VEC criterion for phase boundary prediction seems to work unsatisfactorily for Mn-containing HEA systems [20], which means the different value of VEC criterion for the phase boundary prediction. Co₂₀Cr₂₀Fe₂₀Mn₂₀Ni₂₀ HEAs with VEC of 8.0 have been adequately investigated in recent years [2,4,5,32,33], revealing the TWIP phenomena. With the decrease of Ni content, Co₂₀Cr₂₀Fe_{40-x}Mn₂₀Ni_x (x = 6 at %, 0 at %) HEAs with VEC of 7.72 and 7.6 exhibit the TRIP phenomena [13], which is similar to the Co₃₅Cr₂₅Fe_{40-x}Ni_x (x = 0–15 at %) in this work. A single FCC phase was obtained with the Mn content of 45 at % and 40 at %, and these two alloys exhibit a transition of deformation mechanisms from dislocation slip dominated plasticity to TWIP [3,26]. With the decrease of Mn content, TRIP phenomena were observed in Co₁₀Cr₁₀Fe₄₅Mn₃₅ and Co₁₀Cr₁₀Fe₅₀Mn₃₀. The FCC phase metastability of Co₁₀Cr₁₀Fe_{80-x}Mn_x is enhanced with the decrease of Mn content [3], noting that the VEC of Fe, Mn are 8 and 7, respectively, and VEC value of Co₁₀Cr₁₀Fe_{80-x}Mn_x increased with the decrease of Mn content. Therefore, the transition from TWIP to TRIP based on the VEC criterion in Co₁₀Cr₁₀Fe_{80-x}Mn_x is opposite to the Co₃₅Cr₂₅Fe_{40-x}Ni_x HEAs. Besides, a few additions of Mo and Al reduce the stability of alloys, as well as the VEC value. However, TRIP phenomena do not occur in CoCrFeNiMo_x and Al_xCoCrFeNi systems, based on the published literature [27–30,34,35]. The results indicate that a few additions of Mo and Al do not reduce the value of SFE enough to induce the phase transition during tensile deformation in Co-Cr-Fe-Ni system. More additions of Mo and Al in CoCrFeNi will induce the precipitates from the matrix, which form a multi-phase alloys [36,37]. It is worth noting that the effects of temperature on the SFE is remarkable. The variation of the deformation mechanism from

martensitic transformation to deformation twinning, and to dislocation slip, are observed with the increase of deformation temperature (298 K to 873 K) in the reported TRIP/TWIP steel [38]. It would be useful to investigate the plastic deformation transition temperature in Co-Cr-Fe-Ni systems for potential applications, and more work in this direction is underway.

4. Conclusions

In summary, tensile deformation-induced martensitic transformations occur in $\text{Co}_{35}\text{Cr}_{25}\text{Fe}_{40-x}\text{Ni}_x$ ($x = 15$ at %, 10 at %, 5 at %, 0 at %) HEAs. The excellent combination of tensile strength (760 MPa–1000 MPa) and elongation (65–35%) are attributed to the Co and Cr solid solution strengthening, and the TRIP effect. In non-equal molar Co-Cr-Fe-Ni systems, with a decrease of Ni content, the values of stacking fault energy (SFE) decrease; thus, a TRIP phenomena occurs. Based on the experimental investigation in three different regions of the Co-Cr-Fe-Ni multicomponent phase diagram, the face-centered cubic structured Co-Cr-Fe-Ni HEAs with VEC of ~ 8.0 is more metastable, and TRIP phenomena are more likely to occur. Related results and discussions are useful to the design of a new class of TRIP assisted HEAs.

Author Contributions: F.Y. and X.Z. conceived and designed the experiments; R.C. and P.J. performed the experiments; W.F. wrote the paper. B.L. and X.Q. directed the research and contributed to the discussion and interpretation of the results.

Acknowledgments: This research was supported by the National Science Foundation of China (No. 51701061, 51705129), the Natural Science Foundation of Hebei, China (No. E2016202121), and the National Key Research and Development Program of China (No. 2017-Z02).

Conflicts of Interest: The authors declare no conflict of interest.

References

1. Miracle, D.; Senkov, O. A critical review of high entropy alloys and related concepts. *Acta Mater.* **2017**, *122*, 448–511. [[CrossRef](#)]
2. Gludovatz, B.; Hohenwarter, A.; Catoor, D.; Chang, E.H.; George, E.P.; Ritchie, R.O. A fracture-resistant high-entropy alloy for cryogenic applications. *Science* **2014**, *345*, 1153–1158. [[CrossRef](#)] [[PubMed](#)]
3. Li, Z.; Pradeep, K.G.; Deng, Y.; Raabe, D.; Tasan, C.C. Metastable high-entropy dual-phase alloys overcome the strength-ductility trade-off. *Nature* **2016**, *534*, 227–230. [[CrossRef](#)] [[PubMed](#)]
4. Laplanche, G.; Kostka, A.; Horst, O.M.; Eggeler, G.; George, E.P. Microstructure evolution and critical stress for twinning in the CrMnFeCoNi high-entropy alloy. *Acta Mater.* **2016**, *118*, 152–163. [[CrossRef](#)]
5. Laplanche, G.; Kostka, A.; Reinhart, C.; Hunfeld, J.; Eggeler, G.; George, E.P. Reasons for the superior mechanical properties of medium-entropy CrCoNi compared to high-entropy CrMnFeCoNi. *Acta Mater.* **2017**, *128*, 292–303. [[CrossRef](#)]
6. Zhang, Z.; Mao, M.M.; Wang, J.; Gludovatz, B.; Zhang, Z.; Mao, S.X.; George, E.P.; Yu, Q.; Ritchie, R.O. Nanoscale origins of the damage tolerance of the high-entropy alloy CrMnFeCoNi. *Nat. Commun.* **2015**, *6*, 10143. [[CrossRef](#)] [[PubMed](#)]
7. Huang, S.; Li, W.; Lu, S.; Tian, F.; Shen, J.; Holmström, E.; Vitos, L. Temperature dependent stacking fault energy of FeCrCoNiMn high entropy alloy. *Scr. Mater.* **2015**, *108*, 44–47. [[CrossRef](#)]
8. Miao, J.; Slone, C.E.; Smith, T.M.; Niu, C.; Bei, H.; Ghazisaeidi, M.; Pharr, G.M.; Mills, M.J. The evolution of the deformation substructure in a Ni-Co-Cr equiatomic solid solution alloy. *Acta Mater.* **2017**, *132*, 35–48. [[CrossRef](#)]
9. Liu, S.F.; Wu, Y.; Wang, H.T.; He, J.Y.; Liu, J.B.; Chen, C.X.; Liu, X.J.; Wang, H.; Lu, Z.P. Stacking fault energy of face-centered-cubic high entropy alloys. *Intermetallics* **2018**, *93*, 269–273. [[CrossRef](#)]
10. Lu, S.; Hu, Q.-M.; Johansson, B.; Vitos, L. Stacking fault energies of Mn, Co and Nb alloyed austenitic stainless steels. *Acta Mater.* **2011**, *59*, 5728–5734. [[CrossRef](#)]
11. Wu, Z.; Bei, H.; Pharr, G.M.; George, E.P. Temperature dependence of the mechanical properties of equiatomic solid solution alloys with face-centered cubic crystal structures. *Acta Mater.* **2014**, *81*, 428–441. [[CrossRef](#)]
12. Vaidya, M.; Pradeep, K.G.; Murty, B.S.; Wilde, G.; Divinski, S.V. Bulk tracer diffusion in CoCrFeNi and CoCrFeMnNi high entropy alloys. *Acta Mater.* **2018**, *146*, 211–224. [[CrossRef](#)]

13. Li, Z.; Körmann, F.; Grabowski, B.; Neugebauer, J.; Raabe, D. Ab initio assisted design of quinary dual-phase high-entropy alloys with transformation-induced plasticity. *Acta Mater.* **2017**, *136*, 262–270. [[CrossRef](#)]
14. Li, Z.; Raabe, D. Strong and ductile non-equiatomic high-entropy alloys: Design, processing, microstructure, and mechanical properties. *JOM* **2017**, *69*, 2099–2106. [[CrossRef](#)]
15. Li, Z.; Tasan, C.C.; Pradeep, K.G.; Raabe, D. A trip-assisted dual-phase high-entropy alloy: Grain size and phase fraction effects on deformation behavior. *Acta Mater.* **2017**, *131*, 323–335. [[CrossRef](#)]
16. Zhang, F.; Wu, Y.; Lou, H.; Zeng, Z.; Prakapenka, V.B.; Greenberg, E.; Ren, Y.; Yan, J.; Okasinski, J.S.; Liu, X.; et al. Polymorphism in a high-entropy alloy. *Nat. Commun.* **2017**, *8*, 15687. [[CrossRef](#)] [[PubMed](#)]
17. Otto, F.; Dlouhý, A.; Pradeep, K.G.; Kuběnová, M.; Raabe, D.; Eggeler, G.; George, E.P. Decomposition of the single-phase high-entropy alloy CrMnFeCoNi after prolonged anneals at intermediate temperatures. *Acta Mater.* **2016**, *112*, 40–52. [[CrossRef](#)]
18. Pickering, E.J.; Muñoz-Moreno, R.; Stone, H.J.; Jones, N.G. Precipitation in the equiatomic high-entropy alloy CrMnFeCoNi. *Scr. Mater.* **2016**, *113*, 106–109. [[CrossRef](#)]
19. He, F.; Wang, Z.; Wu, Q.; Li, J.; Wang, J.; Liu, C.T. Phase separation of metastable CoCrFeNi high entropy alloy at intermediate temperatures. *Scr. Mater.* **2017**, *126*, 15–19. [[CrossRef](#)]
20. Guo, S.; Ng, C.; Lu, J.; Liu, C.T. Effect of valence electron concentration on stability of fcc or bcc phase in high entropy alloys. *J. Appl. Phys.* **2011**, *109*, 103505. [[CrossRef](#)]
21. Fang, W.; Chang, R.; Zhang, X.; Ji, P.; Wang, X.; Liu, B.; Li, J.; He, X.; Qu, X.; Yin, F. Effects of cobalt on the structure and mechanical behavior of non-equal molar $\text{Co}_x\text{Fe}_{50-x}\text{Cr}_{25}\text{Ni}_{25}$ high entropy alloys. *Mater. Sci. Eng. A* **2018**, *723*, 221–228. [[CrossRef](#)]
22. Chen, R.; Qin, G.; Zheng, H.; Wang, L.; Su, Y.; Chiu, Y.; Ding, H.; Guo, J.; Fu, H. Composition design of high entropy alloys using the valence electron concentration to balance strength and ductility. *Acta Mater.* **2018**, *144*, 129–137. [[CrossRef](#)]
23. Mizutani, U. Hume-rothery rules for structurally complex alloy phases. *MRS Bull.* **2012**, *37*, 169. [[CrossRef](#)]
24. Lu, J.; Hultman, L.; Holmström, E.; Antonsson, K.H.; Grehk, M.; Li, W.; Vitos, L.; Golpayegani, A. Stacking fault energies in austenitic stainless steels. *Acta Mater.* **2016**, *111*, 39–46. [[CrossRef](#)]
25. Hickel, T.; Sandlöbes, S.; Marceau, R.K.W.; Dick, A.; Bleskov, I.; Neugebauer, J.; Raabe, D. Impact of nanodiffusion on the stacking fault energy in high-strength steels. *Acta Mater.* **2014**, *75*, 147–155. [[CrossRef](#)]
26. Deng, Y.; Tasan, C.C.; Pradeep, K.G.; Springer, H.; Kostka, A.; Raabe, D. Design of a twinning-induced plasticity high entropy alloy. *Acta Mater.* **2015**, *94*, 124–133. [[CrossRef](#)]
27. Cai, B.; Liu, B.; Kabra, S.; Wang, Y.; Yan, K.; Lee, P.; Liu, Y. Deformation mechanisms of Mo alloyed FeCoCrNi high entropy alloy: In situ neutron diffraction. *Acta Mater.* **2017**, *127*, 471–480. [[CrossRef](#)]
28. Liu, J.; Chen, C.; Xu, Y.; Wu, S.; Wang, G.; Wang, H.; Fang, Y.; Meng, L. Deformation twinning behaviors of the low stacking fault energy high-entropy alloy: An in-situ tem study. *Scr. Mater.* **2017**, *137*, 9–12. [[CrossRef](#)]
29. Li, D.; Li, C.; Feng, T.; Zhang, Y.; Sha, G.; Lewandowski, J.J.; Liaw, P.K.; Zhang, Y. High-entropy $\text{Al}_{0.3}\text{CoCrFeNi}$ alloy fibers with high tensile strength and ductility at ambient and cryogenic temperatures. *Acta Mater.* **2017**, *123*, 285–294. [[CrossRef](#)]
30. Joseph, J.; Stanford, N.; Hodgson, P.; Fabijanic, D.M. Tension/compression asymmetry in additive manufactured face centered cubic high entropy alloy. *Scr. Mater.* **2017**, *129*, 30–34. [[CrossRef](#)]
31. Zhang, Y.H.; Zhuang, Y.; Hu, A.; Kai, J.J.; Liu, C.T. The origin of negative stacking fault energies and nano-twin formation in face-centered cubic high entropy alloys. *Scr. Mater.* **2017**, *130*, 96–99. [[CrossRef](#)]
32. Bracq, G.; Laurent-Brocq, M.; Perrière, L.; Pirès, R.; Joubert, J.-M.; Guillot, I. The fcc solid solution stability in the Co-Cr-Fe-Mn-Ni multi-component system. *Acta Mater.* **2017**, *128*, 327–336. [[CrossRef](#)]
33. Laplanche, G.; Bonneville, J.; Varvenne, C.; Curtin, W.A.; George, E.P. Thermal activation parameters of plastic flow reveal deformation mechanisms in the CrMnFeCoNi high-entropy alloy. *Acta Mater.* **2018**, *143*, 257–264. [[CrossRef](#)]
34. Hou, J.; Zhang, M.; Yang, H.; Qiao, J. Deformation behavior of $\text{Al}_{0.25}\text{CoCrFeNi}$ high-entropy alloy after recrystallization. *Metals* **2017**, *7*, 111. [[CrossRef](#)]
35. Lindner, T.; Loebel, M.; Mehner, T.; Dietrich, D.; Lampke, T. The phase composition and microstructure of $\text{Al}_x\text{CoCrFeNiTi}$ alloys for the development of high-entropy alloy systems. *Metals* **2017**, *7*, 162. [[CrossRef](#)]
36. Shun, T.-T.; Chang, L.-Y.; Shiu, M.-H. Microstructure and mechanical properties of multiprincipal component CoCrFeNiMo_x alloys. *Mater. Charact.* **2012**, *70*, 63–67. [[CrossRef](#)]

37. Saal, J.E.; Berglund, I.S.; Sebastian, J.T.; Liaw, P.K.; Olson, G.B. Equilibrium high entropy alloy phase stability from experiments and thermodynamic modeling. *Scr. Mater.* **2018**, *146*, 5–8. [[CrossRef](#)]
38. Yin, F.X.; Xia, H.; Feng, J.H.; Cai, M.H.; Zhang, X.; Wang, G.K.; Sawaguchi, T. Mechanical properties of an Fe-30Mn-4Si-2Al alloy after rolling at different temperatures ranging from 298 to 1073 k. *Mater. Sci. Eng. A* **2018**, *725*, 127–137. [[CrossRef](#)]



© 2018 by the authors. Licensee MDPI, Basel, Switzerland. This article is an open access article distributed under the terms and conditions of the Creative Commons Attribution (CC BY) license (<http://creativecommons.org/licenses/by/4.0/>).